ORIGINAL ARTICLE

Traffic WILEY

Biogenesis of large dense core vesicles in mouse chromaffin cells

Ekta Dembla | Ute Becherer

Cellular Neurophysiology, CIPMM, Saarland University, Homburg, Germany

Correspondence
Ute Becherer, Cellular Neurophysiology, Center for Integrative Physiology and Molecular Medicine (CIPMM), Saarland University, 66424 Homburg, Germany.
Email: ute.becherer@uks.eu

Present address
Ekta Dembla, Department of Neuroanatomy, Institute for Anatomy and Cell Biology, Saarland University, Homburg, Germany

Abstract

Large dense core vesicle (LDCVs) biogenesis in neuroendocrine cells involves: (a) production of cargo peptides processed in the Golgi; (b) fission of cargo loaded LDCVs undergoing maturation steps; (c) movement of these LDCVs to the plasma membrane. These steps have been resolved over several decades in PC12 cells and in bovine chromaffin cells. More recently, the molecular machinery involved in LDCV biogenesis has been examined using genetically modified mice, generating contradictory results. To address these contradictions, we have used NPY-mCherry electroporation combined with immunolabeling and super-resolution structured illumination microscopy. We show that LDCVs separate from an intermediate Golgi compartment, mature in its proximity for about 1 hour and then travel to the plasma membrane. The exocytotic machinery composed of vSNAREs and synaptotagmin1, which originate from either de novo synthesis or recycling, is most likely acquired via fusion with precursor vesicles during maturation. Finally, recycling of LDCV membrane protein is achieved in less than 2 hours. With this comprehensive scheme of LDCV biogenesis we have established a framework for future studies in mouse chromaffin cells.

KEYWORDS
biogenesis, chromaffin cell, granule, recycling, structure illumination microscopy

1 | INTRODUCTION

Large dense core vesicles (LDCVs) are present in a variety of secretory cells. They are the storage organelles for peptidergic and amine hormones that are released on demand. In chromaffin cells they contain adrenalin and noradrenalin, a large variety of peptides such as neuropeptide Y (NPY) and natriuretic peptides, and matrix proteins such as chromogranin (for review see reference[1]). LDCVs are released via SNARE-mediated exocytosis, upon splanchnic nerve stimulation. Biogenesis of LDCVs consists of several steps. First, the secretory cargo proteins composed of dense core matrix proteins and neuropeptides

are produced. They aggregate in the trans-Golgi network (TGN) from which immature dense core vesicles containing the cargo and membrane proteins such as synaptobrevin, cellubrevin, GP III bud off.[2] Finally, these newly generated LDCVs appear to move rapidly toward the plasma membrane[3] and further mature while loading with catecholamine. LDCV membrane proteins can be recycled after exocytosis and appear in newly formed LDCVs within 45 minutes without passing through the TGN.[4] This scheme of LDCV biogenesis has been generated over several decades using a large array of techniques such as pulse-chase experiments in combination with electron microscopy (EM),[4] subcellular fractionation,[5] and over-expression of chromogranin

labeled with fluorescent proteins.[2,3] Some of these experiments were performed on bovine chromaffin cells but most were carried out in PC12 cells, which are derived from a pheochromocytoma of the rat adrenal medulla and thus resemble but are not identical to rat chromaffin cells.

In recent years, new efforts have been made to understand the molecular mechanisms regulating LDCV biogenesis. The role of granins in aggregation of the secretory components and in catecholamine loading of LDCV has been intensely scrutinized (reviewed in reference[6,7]). Using the availability of genetically engineered mice, a new set of proteins that are involved in LDCV component sorting and trafficking, such as Vti1a and PICK1, were investigated in mouse chromaffin cells.[8,9] These experiments revealed that the sorting of vesicular SNAREs (vSNAREs), which are LDCV membrane components, occurs very late in the biogenesis of LDCVs, and as much as 12 hours after leaving the TGN. This is in contradiction with other studies in which sorting of synaptophysin to LDCVs was shown to occur in less than 1 hour after leaving the TGN in PC12 cells.[2] However, these studies were performed on different cell types and using different techniques. Because ability to generate genetically engineered mice became increasingly easier, more studies on the molecular mechanism of LDCV biogenesis will be possible, thus it is essential to determine the chronological sequence of LDCV biogenesis in mouse chromaffin cells. We investigated this process using overexpression of NPY tagged to the fluorescent protein mCherry to label newly generated LDCVs, in combination with immunofluorescence and high-resolution microscopy, to study their co-localization with various sub-cellular markers. We found that LDCVs originate from an intermediate Golgi compartment and that they mature in close proximity to the Golgi for about 1 hour before they move toward the plasma membrane. During maturation, vesicular SNAREs (vSNAREs) and synaptotagmin1, which originate from de novo synthesis or from a recycling pathway, are inserted into LDCV membrane. This most likely occurs via fusion with precursor vesicles. Finally, we show that the recycling of synaptotagmin1 to immature LDCV takes a minimum of 1 hours.

2 | RESULTS

2.1 | LDCVs are retained in close proximity to the Golgi for about 1 hour before moving toward the plasma membrane

Our aim was to follow the biogenesis of LDCVs in mouse chromaffin cells using NPY-mCherry electroporation as a chase like type of experimental approach. The advantages of this transfection method in comparison to virus based transfection is that the exact time point of transfection is known and the physiology of successfully transfected cells is less affected allowing us to observe the cells for several days. Throughout this study the cells were observed with structured illumination microscopy (SIM) to obtain a very high resolution in three dimensions permitting detailed observation of the co-localization of

proteins (Figure S1).[10,11] NPY-mCherry has been used extensively to specifically mark LDCVs in bovine chromaffin cells but not in mouse cells.[12,13] With anti-chromogranin A (CgA) antibody as a marker for LDCVs and anti-LAMP1 antibody as a marker for lysosomes, we confirmed that NPY-mCherry containing vesicles were LDCVs (Figure S2). Pearson's correlation coefficient was 0.51 ± 0.02. Manders coefficient for CgA overlapping with NPY-mCherry was 0.6 ± 0.03 and for NPY-mCherry overlapping with CgA was 0.6 ± 0.02 (n = 15), which indicated good co-localization between CgA and NPY (Figure S2B). Some CgA puncta did not overlap with NPY, because LDCVs generated before NPY-mCherry transfection were not labeled with mCherry. In addition, NPY-mCherry fluorescence did not completely co-localized to CgA because a significant portion of the NPY-mCherry was found in the Golgi (Figure S2A). The Pearson's correlation coefficient of anti-LAMP1 antibody and NPY-mCherry were equal to 0.18 ± 0.01, and below 0.1 for both Manders coefficient (n = 15; Figure S2D) indicating no correlation between LAMP1 and NPY. Thus, NPY-mCherry was clearly localized to LDCVs and not lysosomes.

To follow the fate of the newly synthesized vesicles, we fixed NPY-mCherry transfected cells at different time points after transfection, immuno-labeled them with the cis-Golgi marker GM130 and used the cortical actin network marker phalloidine-Alexa488 to delineate the cell border (Figure 1). We acquired a set of 10 cells at each time point. The earliest NPY-mCherry fluorescence was visible 2 hours after transfection and was exclusively localized to the immediate vicinity of the cis-Golgi (Figure 1, first row). Very few individual vesicles were present indicating that 2 hours is the minimum time required to generate LDCVs. One hour later, LDCVs were observed in the cytoplasm, with few having reached the cortical actin network adjacent to the plasma membrane (Figure 1, row 2). At later time points increasing numbers of vesicles were observed, which were distributed throughout the cytoplasm and adjacent to the plasma membrane.

To analyze the localization of newly synthesized vesicles, we measured the distance between the center of the vesicles and the border of the cis-Golgi or the plasma membrane and displayed the distance distributions as histograms (Figure 2). In the first 2 hours all LDCVs were found next to the cis-Golgi (Figure 2A), though in some cases in which the Golgi was near the plasma membrane, vesicles also appeared close to the plasma membrane. There were 34.9 ± 3.2 vesicles within 250 nm of the cis-Golgi at 2 hours. Following a decline to 18.0 ± 3.2 vesicles after 3 hours, the number of vesicles within 250 nm of the cis-Golgi increased to 23.9 ± 7.4 at 4 hours, and reached a maximum of 46.1 ± 7.0 at 8 hours. The number of vesicles adjacent to the Golgi remained relatively constant after 8 hours (Figure 2H). The biphasic LDCV generation was probably due to cell-stress by the isolation procedure and electroporation, possibly leading to a reduced protein production at initial time points. The number of vesicles located near the plasma membrane also increased slowly over time.

To analyze this in more detail we counted the number of LDCVs located in the cortical actin ring. Its thickness was about 430 nm,
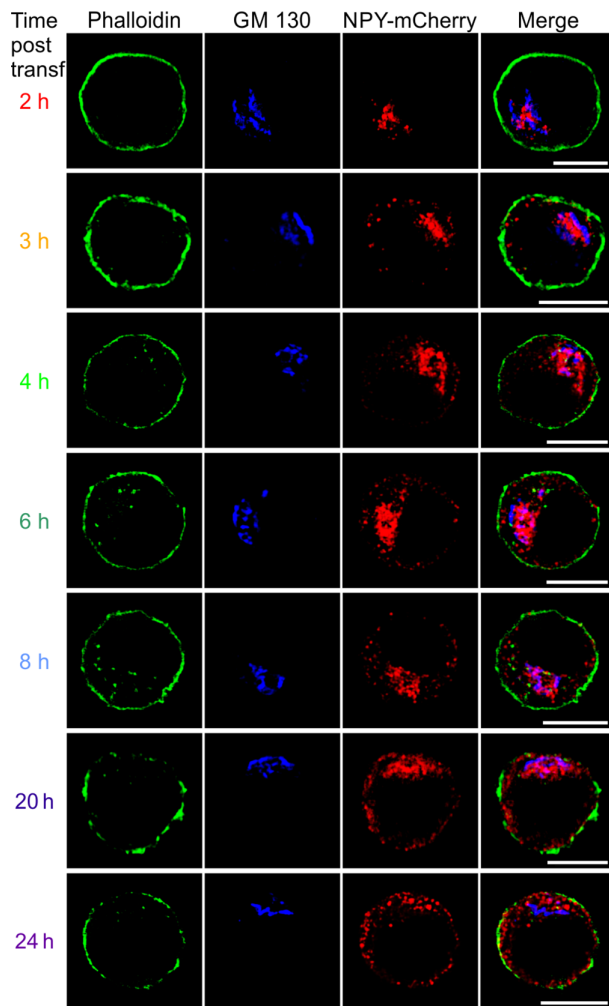
FIGURE 1 Time course of LDCV biogenesis. Chromaffin cells were transfected with NPY-mCherry (red) and maintained in culture for the times indicated on the left of the images. After fixation, the cortical actin network was labeled with Phalloidin-Alexa488 (green) and the cis-Golgi network was labeled with anti-GM130 antibody (blue). Displayed are representative central single plane SIM images in which the cis-Golgi is visible. Scale bars: 5 μm

which corresponded to the full width at half-maximum of an intensity profile plot running perpendicular to the actin cortex on the SIM processed images. LDCVs located in the actin cortex are highlighted with a gray background in the histograms (Figure 2A-G). Although newly generated vesicles appear to accumulate in the cortical actin ring they do not seem to be retained there since within 6 hours of transfection they represent less than 30% of all red-labeled LDCVs (Figure 2H). Hence, most red-labeled LDCVs are equally distributed in the cytoplasm. Furthermore, the number of LDCVs retained right at the plasma membrane (first bin of the histogram) seemed stable over time. In contrast, the number of labeled LDCVs located in the inner part of the actin cortex, that is, located at a distance between 250 and 500 nm from the plasma membrane (second bin of the histogram), increased from 4.6 ± 1.3 after 2 hours to 46.7 ± 4.0 vesicles after 24 hours.

In addition to the accumulation of LDCVs at the plasma membrane, we observed a strong red staining including elongated structures in the vicinity of the Golgi throughout the experiment. It co-localized with the cis-Golgi marker anti-GM130 only to a minor degree (Figure 1), which is consistent with previous results.[2] One possible explanation for this relative lack of cis-Golgi staining is that NPY-mCherry proceeds through cis-Golgi cisternae in less time than it takes for mCherry fluorescence to mature (15 to 40 minutes,[14,15]). However, the red fluorescent staining of elongated structures clearly did not correspond to LDCVs as it was not stained by a CgA antibody (Figure S2). Thus, we wondered if it corresponded to the TGN.

2.2 | Early NPY-mCherry expression identifies a distinct cellular compartment

To address this question, we performed a co-immunolabeling of the cis- and trans-Golgi network in NPY-mCherry (red) transfected chromaffin cells at three different time points (Figure 3A). TGN38 has been used extensively as a marker for the TGN. In cell lines such as PC12 cells anti-TGN38 labels only elongated cisternae like structures.[16,17] In addition to cisternae-like structures, we observed labeled small vesicle-like organelles that were widely distributed in the cytoplasm (Figure 3A). These vesicles did not correspond to LDCVs since they did not contain NPY-mCherry. TGN38 partially co-localized with NPY-mCherry when it was located close to the cis-Golgi. We quantified the co-localization of TGN38 and GM130 with NPY-mCherry by Pearson's coefficients and Manders coefficients for 15 cells in two ways: one analysis encompassed the whole cell (Figure S3A,B) and the second analysis was restricted to an area near the Golgi in order to avoid interference of vesicular TGN38 labeling (Figure 3B,C). For example, the Manders coefficient, in which the co-localization of TGN38 to NPY-mCherry was analyzed on the whole cell, was much smaller than the coefficient that was measured on an area near the Golgi (Figure S3B and 3C). This is because the vesicular fraction of TGN38 is impacting the co-localization analysis made on the whole cell.

Pearson's correlation coefficients revealed a very low co-localization between NPY and TGN38 or GM130 with values below 0.3 at all the three time points whether the analysis included the whole cell or was restricted to the Golgi. However, both analyses showed that co-localization of NPY-mCherry with GM130 steadily decreased while there was a transient increase in co-localization between NPY-mCherry and TGN38 at 3 hours post transfection (Figure S3A and 3B). This change over time might reflect the progression of NPY-mCherry from cis- to trans-Golgi. Furthermore, the Manders coefficient measurement restricted to the Golgi area produced higher co-localization of the Golgi markers to NPY-mCherry than of NPY-mCherry to the Golgi markers (Figure 3C). This indicates that a large fraction of NPY-mCherry that is located near the Golgi is neither localized to the cis nor the trans-Golgi network revealing a separate Golgi compartment. To better define this compartment, we plotted the intensity profile of NPY-mCherry (red), TGN38 (green),
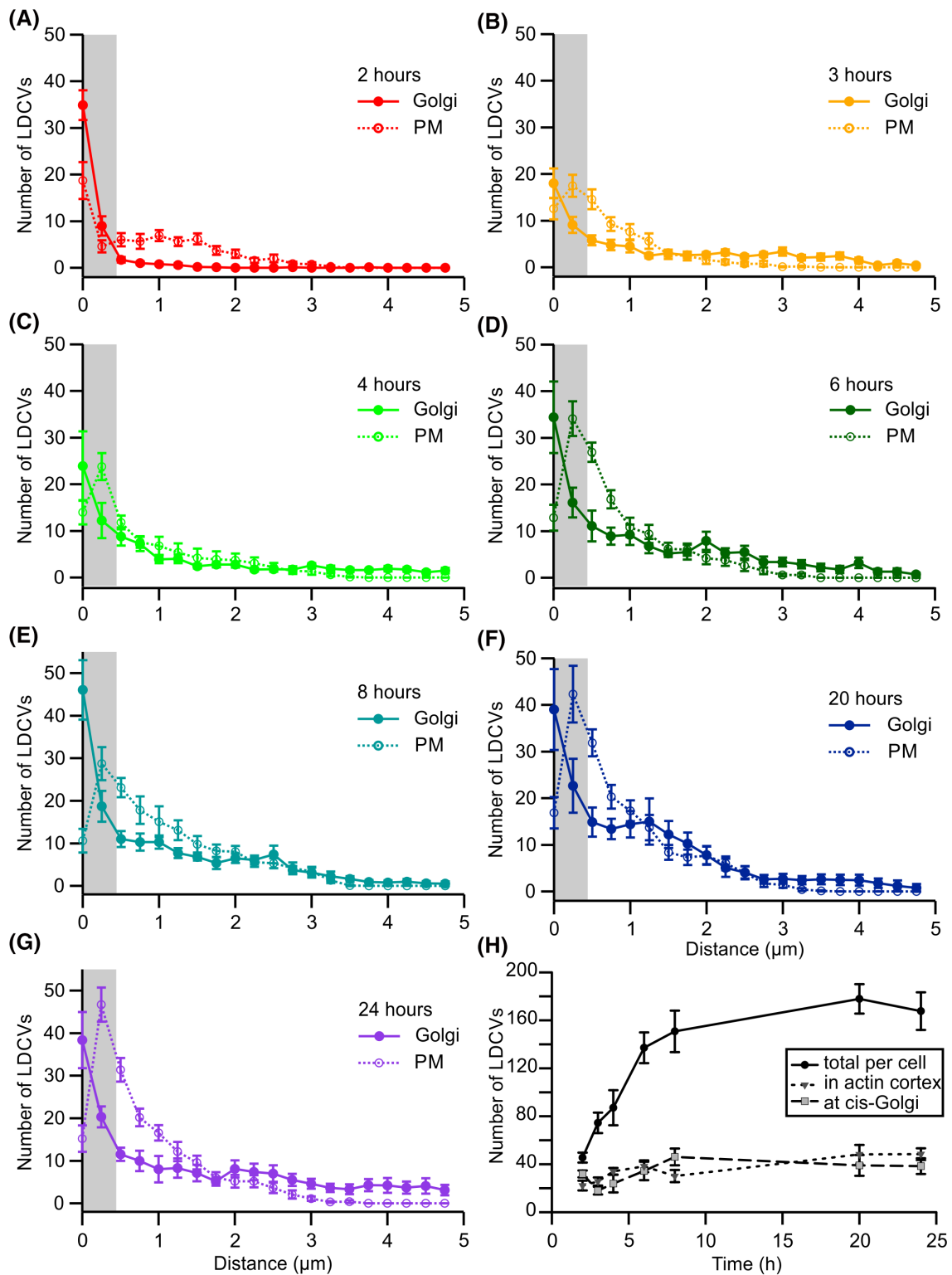
FIGURE 2 LDCVs exit the Golgi only 2 hour after first expression of NPY-mCherry. A-G, Localization of LDCVs in cells as shown in Figure 1 was analyzed. Their distance to the cis-Golgi (solid line with filled circle) and the plasma membrane (PM, dotted line with empty circle) is displayed as an average histogram for various time points after transfection (2 hours, A, 3 hours, B, 4 hours, C, 6 hours D, 8 hours, E, 20 hours, F, and 24 hours, G). H, Time course of the LDCV number in the entire cell slice (solid line), in the Actin cortex, that is, within 430 nm of the plasma membrane (stippled line), and within 250 nm of the Golgi (dashed line). Plotted are average number of LDCVs ± SEM (n = 10 cells for each time point)
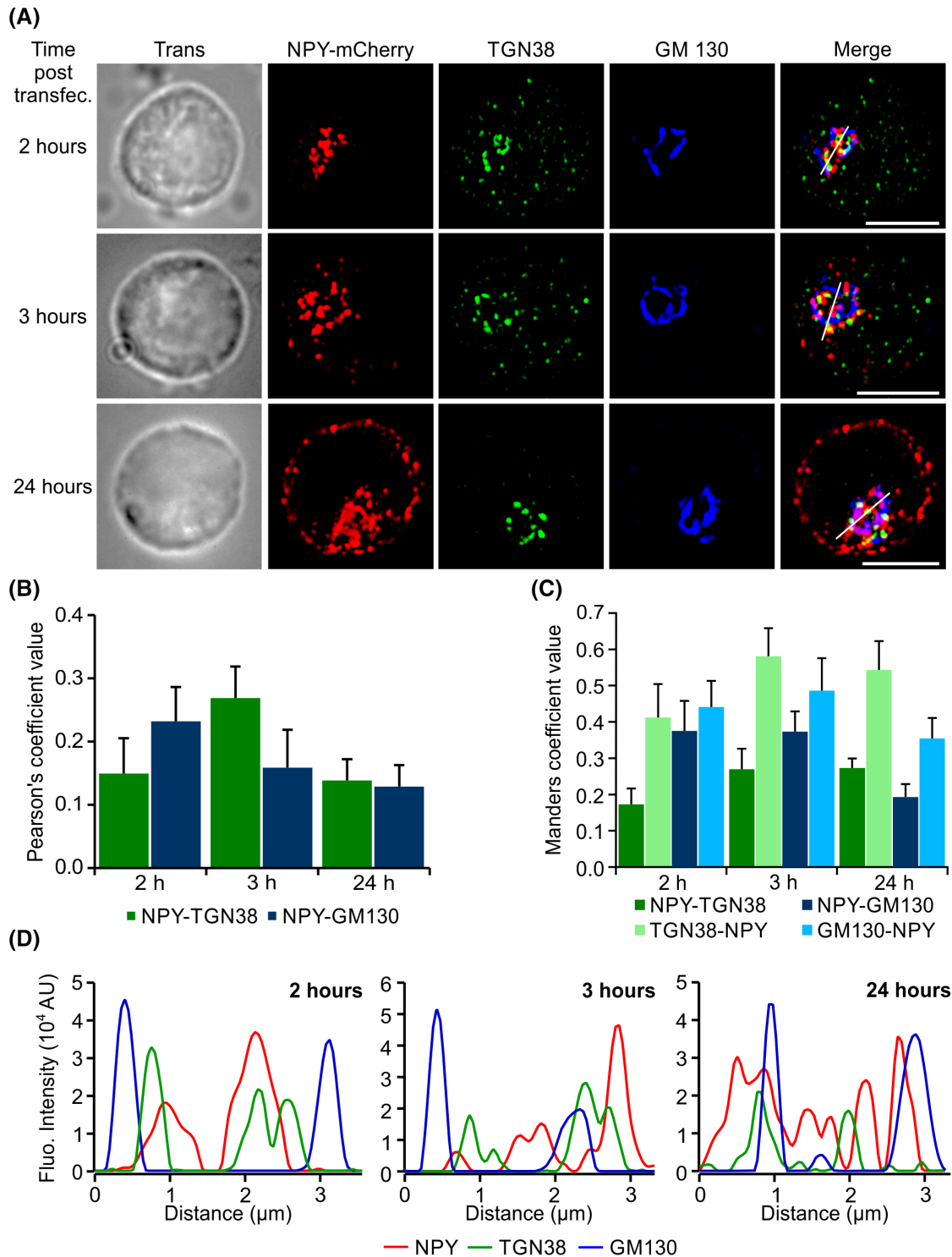
(A)

FIGURE 3 NPY-mCherry partially overlaps with cis- and trans-Golgi network. A, Single plane SIM images of NPY-mCherry (red) transfected chromaffin cells maintained in culture for varying times indicated on the left of the images. After fixation, the cells were immunolabeled with Golgi markers; TGN38 (green) for trans-Golgi, and GM130 (blue) for cis-Golgi network. Scale bars: 5 μm. B, Co-localization between NPY, TGN38 and GM130 close to the Golgi was analyzed with Pearson's coefficients. C, Manders co-localization coefficients between NPY, TGN38 and GM130 measured on an area close to the Golgi. Average co-localization coefficients are shown ± SEM (n = 7 cells for each time point). D, Intensity profiles of NPY (red), TGN38 (green), and GM130 (blue) analyzed across the white line shown in the merge images in A

and GM130 (blue) across the white line shown in the merged images of exemplary cells in Figure 3A. We observed high fluorescence intensity of NPY-mCherry when GM130 and TGN38 signal was close to zero at all three time points (Figure 3D). This result furthers our hypothesis of a separate Golgi compartment that harbors NPY-mCherry yet to be loaded into vesicles.

It has been suggested that LDCVs are generated from a syntaxin6 positive or a Golgin97 positive structure known to be a TGN sub-compartment.[2,9] To verify that hypothesis we performed co-immunolabeling with the anti-GM130 to mark the cis-Golgi and an anti-syntaxin6 antibody. Similar to GM130 and TGN38, NPY-mCherry co-localization with syntaxin6 measured with Pearson's coefficient was low (Figure 4B). However, syntaxin6 co-localized with NPY-mCherry on discrete spots in the Golgi that are devoid of GM130 staining. This is clearly visible on the line plot analysis performed over the Golgi of exemplary cells (Figure 4C) and is reflected by an average Manders coefficient of 0.44 ± 0.01 (n = 10 for each time point) for NPY-mCherry localizing to Syntaxin6. Manders and Pearson's coefficients are quite stable over time indicating that the proportion of NPY that proceeded through the synatxin6 positive TGN sub-compartment remains constant.

Work from Park et al.[2] suggested that LDCV membrane protein such as synaptobrevin are associated with the LDCVs as they bud out of a TGN sub-compartment. However, Walter et al.[9] and Pinheiro et al.[8] hypothesized that LDCVs emerge from the TGN without the vSNAREs synaptobrevin and cellubrevin, and that they associate with them at later stage. We shed light on this contradiction by performing a variety of co-immunolabeling.

2.3 | Vesicular SNAREs and synaptotagmin1 are sorted to LDCVs at a late time point in the biogenesis of LDCVs

If NPY-mCherry loaded vesicles emerging from the TGN sub-compartment are fully functional LDCVs then their membrane must contain the vSNARE proteins synaptobrevin-2 and cellubrevin, the Ca^{2+}-sensor for exocytosis synaptotagmin1, a vesicular monoamine transporter to load the vesicle with catecholamine, and so forth. In addition, these proteins must be present in the TGN sub-compartment. However, it is also possible that LDCV membrane proteins are located on endosomes and associate with LDCV precursors that contain the cargo at a later stage by intracellular fusion of two vesicles. In this case the TGN sub-compartment and some NPY-mCherry loaded
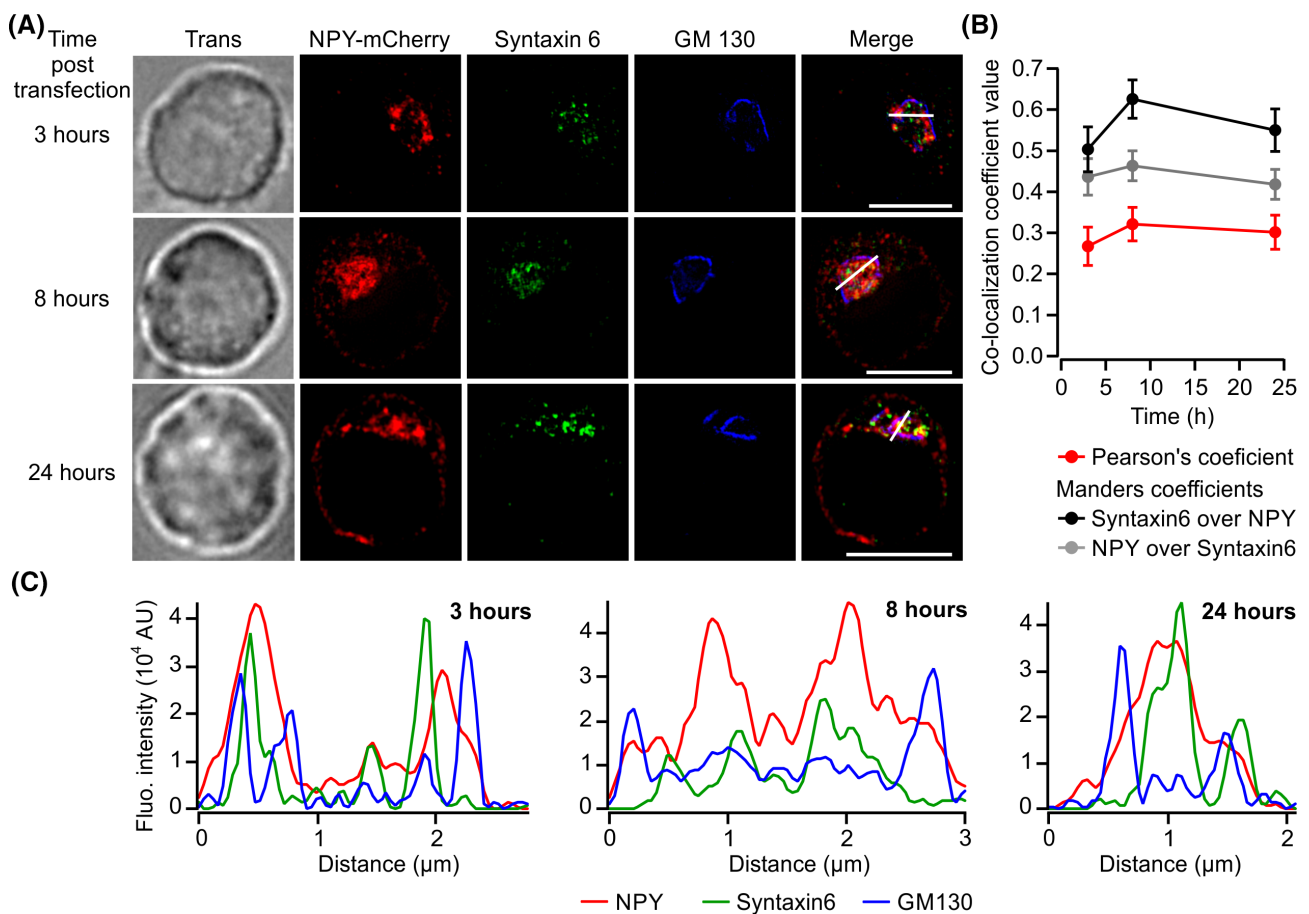

FIGURE 4 NPY-mCherry transit through a syntaxin6 positive trans-Golgi sub-compartment. A, Single plane SIM images of NPY-mCherry (red) transfected chromaffin cells maintained in culture for varying times indicated on the left of the images. After fixation, the Golgi was immunolabeled with anti-syntaxin6 (green) and anti-GM130 (blue). Scale bars: 5 μm. B, The co-localization between NPY, syntaxin6 and GM130 in vicinity of the Golgi was analyzed with Pearson's and Manders co-localization coefficients. Average co-localization coefficients are shown ± SEM (n = 10 cells for each time point). C, Intensity profiles of NPY (red), syntaxin6 (green), and GM130 (blue) that were analyzed across the white line shown in the merge images in, A

vesicles would contain neither vSNAREs nor the other vesicular membrane proteins. To distinguish between these two possibilities, we performed NPY-mCherry transfection in conjunction with a full set of immunolabeling.

We fixed chromaffin cells transfected with NPY-mCherry (red) at different time points after transfection then immunolabeled them with anti-synaptobrevin2 (Figure 5), anti-cellubrevin (Figure 6), and anti-synaptotagmin1 (Figure 7) antibodies. As can be seen from pictures of representative cells, all three proteins are localized to discrete spots mainly in direct vicinity of the plasma membrane but also in the cytoplasm (Figures 5A, 6A and 7A). At 2 hours, very few spots of synaptobrevin2, cellubrevin, and synaptotagmin1 overlap with NPY-mCherry staining. We then analyzed co-localization of NPY-mCherry with one of the above cited proteins on single image plane devoid of Golgi to focus the analysis on LDCVs. At 2 hours, all Pearson's and Manders coefficients between NPY-mCherry and the three vesicular proteins were below 0.25 indicating negligible co-localization at this time point. If the vesicular proteins are added to newly generated vesicles directly from the Golgi then co-localization values should be high at an early stage as can be seen from the Manders coefficient of NPY-mCherry with another soluble cargo such as CgA (Figure S2).

We furthered this analysis by counting the number of vSNARE or synaptotagmin1 positive puncta that overlapped with NPY-mCherry near the Golgi over the entire z-stack of cells fixed 2 hours after transfection. Out of 34.9 ± 3.2 NPY-mCherry positive puncta (Figure 2), we found that an average of only 4.2 ± 0.5, 5.1 ± 0.6 and 3.9 ± 0.6 were also positive for synaptobrevin2, cellubrevin, and synaptotagmin1, respectively (panel C of Figures 5, 6 and 7 respectively, n = 15). In addition, short-term co-transfection of NPY-Venus and synaptobrevin2-RFP in cells only led to their partial co-localization at discrete spots (Figure S4). These results support the hypothesis that vesicular membrane proteins are not loaded on newly synthesized vesicles at the time when they exit the Golgi. After longer delay the degree of co-localization increased. Three hours after transfection slightly more individual spots of vesicular proteins overlapped with NPY-mCherry and after 8 hours there was a sudden increase in the co-localization as can been seen from the yellow spots on the merged images of representative cells. Highest co-localization between NPY-mCherry and the vesicular proteins was measured at 24 hours after transfection. Pearson's coefficients reached values of 0.57 ± 0.03, 0.33 ± 0.01, 0.51 ± 0.03 for synaptobrevin2, cellubrevin and synaptotagmin1 respectively (panel B of Figures 5, 6 and 7; n = 15 for all time points and staining). This increasing co-localization over time was not observed between NPY-mCherry and CgA (Figure S2) indicating that vesicular membrane proteins are probably sorted to LDCV independently from its soluble cargo. Co-localization of synaptobrevin2 and synaptotagmin1 with NPY-mCherry was higher than that of cellubrevin. We wondered whether LDCVs devoid of synaptobrevin2 contained cellubrevin and if all NPY-mCherry labeled vesicles were vSNARE positive. A double immunolabeling with anti-synaptobrevin2 (green) and anti-cellubrevin (blue) of chromaffin cells maintained in culture for 24 hours after transfection showed that this was not the case (Figure 6D). The co-localization between both
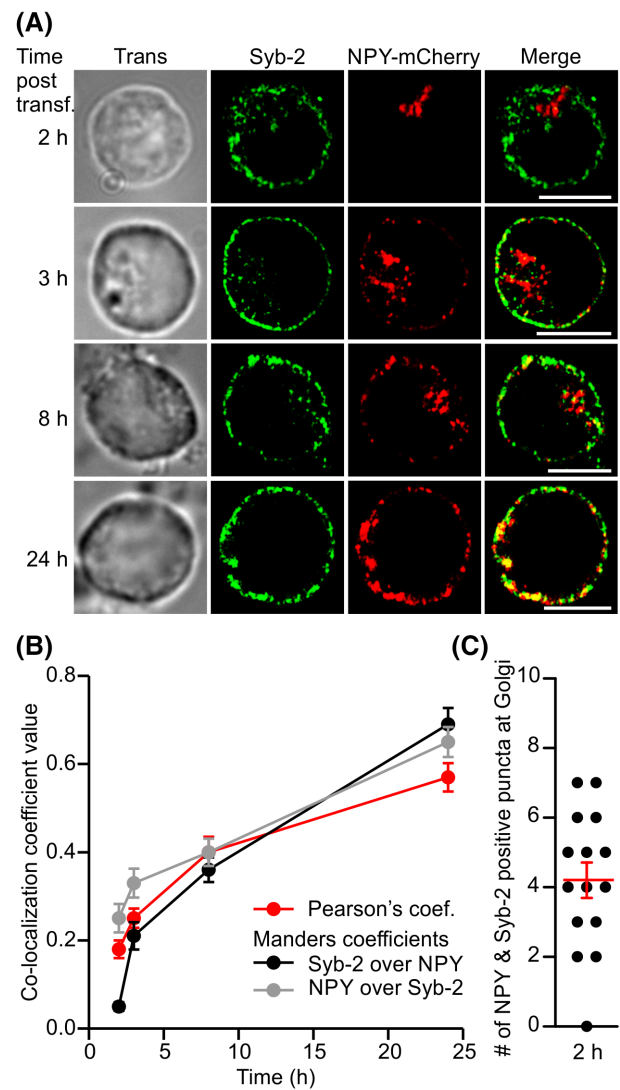

FIGURE 5 Synaptobrevin2 is associated with LDCVs at a late stage of biogenesis. A, Chromaffin cells transfected with NPY-mCherry (red) were maintained in culture for the time indicated on the left of the images. After fixation, cells were immunolabeled with anti-synaptobrevin2 antibody (Syb2, green). Representative single plane images were acquired by SIM. B, Co-localization between NPY-mCherry and synaptobrevin2 over time. Pearson's coefficient and Manders coefficients were analyzed for each time point from two different experiments (n = 15 cells for each time point). Plotted are average co-localization coefficients ± SEM. C, Scatter dot plot of the number of puncta per cell in which synaptobrevin2 and NPY-mCherry co-localized. Measured are cells fixed 2 hours after transfection. The puncta were quantified over the entire 3D stack in vicinity of NPY-mCherry positive structures typical for the Golgi. Average ± SEM is presented as red lines. Scale bars: 5 μm

vSNAREs was 0.58 ± 0.03 (Figure 6E; n = 15, Pearson's coefficient), which is below a previously reported value.[18] This discrepancy most likely arises because the vSNAREs were not overexpressed in our experiments and our analysis was not restricted to the proximity of the plasma membrane. The co-localization coefficients of NPY-mCherry with both vSNAREs were measured by merging the blue and

green channels and comparing this merged image with the red channel of NPY-mCherry. The Manders coefficient of NPY-mCherry localized to both vSNAREs was 0.68 ± 0.03 (Figure 6F), which is similar to 0.65 ± 0.03 for the Manders of NPY-mCherry localized to

synaptobrevin2 alone. This means that some red labeled vesicles are devoid of vSNAREs. Since no co-localization with LAMP1 was found (Figure S2), these red vesicles cannot be lysosomes containing degradation products of NPY-mCherry but they are rather intermediate LDCV-precursors that are devoid of the fusion machinery.

Our data strongly suggest that fully functional LDCVs are not directly generated by fission from the TGN but arise from the fusion of LDCV-precursor with vesicles containing vSNAREs and synaptotagmin1. If that is the case then these proteins might originate from recycling of LDCV membrane after exocytosis rather than from de novo synthesis. We tested this possibility by following synaptotagmin1 recycling.

2.4 | Synaptotagmin1 joins NPY-mCherry loaded vesicles within 2 hours after endocytosis and is processed independently of recycling endosomes

To study the endocytosis and recycling of synaptotagmin1 in chromaffin cells expressing NPY-mCherry for 24 hours, we incubated the cells with an antibody directed against the lumenal domain of synaptotagmin1, while exocytosis was stimulated for 5 minutes with a solution containing 60 mM KCl. Control cells were subjected to normal extracellular solution in the presence of the antibody. This was followed or not by a recovery phase at 37°C with 13% CO_2, which lasted between 30 minutes and 6 hours (Figure 8A). Then the cells were immediately fixed and processed for secondary antibody application. We verified that synaptotagmin1 was reliably labeled with its
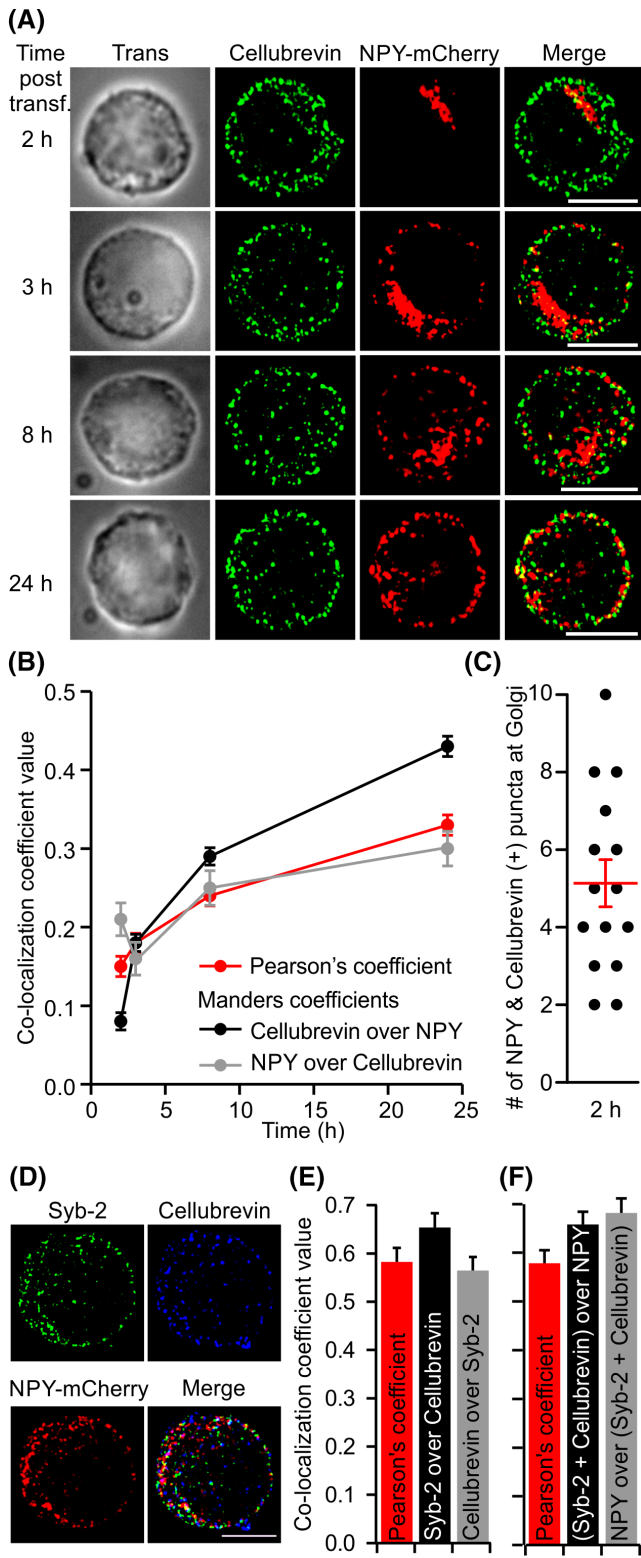

FIGURE 6 Cellubrevin is localized to a relatively small population of LDCVs. A, Single plane SIM images of chromaffin cells transfected with NPY-mCherry (red) and maintained in culture for varying times as described on the left-hand side of the images. After fixation, cells were labeled with anti-cellubrevin antibody (green). B, Co-localization between NPY-mCherry and cellubrevin over time. Pearson's coefficient and Manders coefficients were analyzed for each time point from two independent experiments (n = 15 cells for each time point). C, Scatter dot plot of the number of puncta per cell in which cellubrevin and NPY-mCherry co-localized. Measured are cells fixed 2 hours after transfection. The puncta were quantified in 3D in vicinity of the Golgi. Average ± SEM is presented as red lines. D, Single plane images of chromaffin cell transfected with NPY-mCherry (red) and maintained in culture for 24 hours before immunolabeling with anti-synaptobrevin2 (Syb2, green) and anti-cellubrevin (blue). Note that native synaptobrevin and cellubrevin are not perfectly co-localized. E, Co-localization analysis between synaptobrevin2 and cellubrevin shown as Pearson's coefficient (red), Manders coefficient for synaptobrevin2 overlapping with cellubrevin (black), and Manders coefficient for cellubrevin overlapping with synaptobrevin2 (gray) (n = 15 cells). F, Co-localization analysis between NPY-mCherry and both vSNAREs combined shown as Pearson's coefficient (red), Manders coefficient for vSNAREs overlapping with NPY-mCherry (black), and Manders coefficient for NPY-mCherry overlapping with combined vSNAREs (gray) (n = 15 cells). Presented are the average co-localization coefficients ± SEM. Scale bars are 5 μm
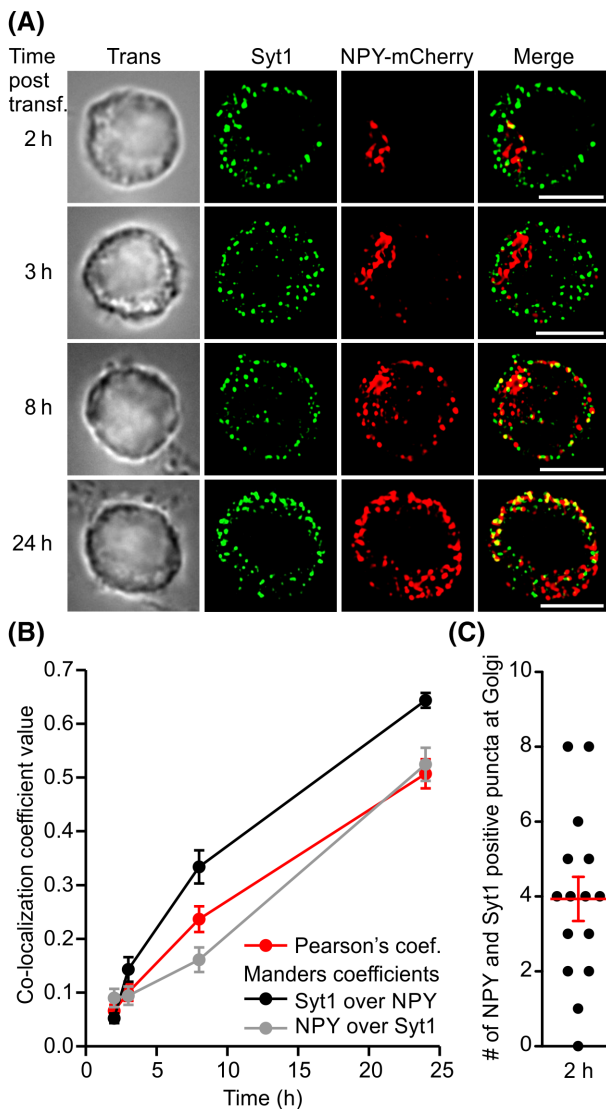
(A)

FIGURE 7 Like vSNAREs, synaptotagmin1 is sorted to LDCVs at a late stage of their biogenesis. A, NPY-mCherry (red) transfected chromaffin cells were maintained in culture for varying times as shown on the left of the images. After fixation, cells were immunolabeled with anti-synaptotagmin1 antibody (Syt1, green). Representative single plane images were acquired by SIM. Scale bars: 5 μm. B, Displayed is the co-localization study between NPY-mCherry and cellubrevin over time. Pearson's coefficient and Manders coefficients were analyzed for each time point from two different experiments (n = 15 cells for each time point). Presented are average co-localization coefficients ± SEM. C, Scatter dot plot of the number of puncta in which synaptotagmin1 and NPY-mCherry co-localized per cell fixed 2 hours after transfection. The puncta were quantified in 3D in vicinity of the Golgi. Average ± SEM is presented as red lines

antibody during recycling through lysosomes (Figure S5A-C), and that the low pH of lysosome does not dissociate the antibody from its target (Figure S5D,E). We also tested that antibody uptake occurs neither in unstimulated cells nor through bulk endocytosis (Figure S5F, G). We found that when the cells were not allowed to recover after stimulation (time point 0 min) then the antibody staining was entirely confined to the surface of the cell (Figure 8B). Allowing recovery time

resulted in a strong reduction in the number of puncta at the plasma membrane, while the overall number of puncta in the entire cell remained roughly constant (Figure 8C). Retrieval of endocytosed synaptotagmin1 vesicles into the cytoplasm occurred in 30 minutes after stimulation. However, at that time point no synaptotagmin1 positive puncta were co-localized with NPY-mCherry. Co-localization of endocytosed synaptotagmin1 with NPY-mCherry was visible after 2 hours (6 ± 0.7 puncta in which both marker co-localize). This co-localization did not result from vesicle crowding near the Golgi as both markers, NPY-mCherry and endocytosed anti-synaptotagmin1 antibody were observed to move together in live cells (Figure S5H). After a delay of 6 hours the amount of synaptotagmin1 puncta associating with NPY-mCherry increased to 13.2 ± 2.89 (n = 5).

We counted synaptotagmin1 puncta at the membrane at different times to see if after recycling, LDCVs loaded with endocytosed synaptotagmin1 eventually move back to the plasma membrane (Figure 8C). Yet even after 6 hours of recovery synaptotagmin1 puncta appeared evenly distributed in the cytoplasm, whether they were co-localized with NPY-mCherry or not (Figure 8C). Furthermore, synaptotagmin1 puncta did not seem to aggregate close to the Golgi at a place where fusion of LDCV-precursor and synaptotagmin recycling vesicles might take place (Figure 8B).

To investigate the subcellular localization of endocytosed synaptotagmin1 in more details we used the previous protocol to stain recycling synaptotagmin1 and compared its localization to the TGN using anti-TGN38 as marker (Figure 9A). The recovery time was set to 2 and 3 hours because these were the first time points at which recycling synaptotagmin1 was co-localized with NPY-mCherry, suggesting that recycled synaptotagmin1 is transferred from endosomes to newly generated LDCVs. Endocytosed synaptotagmin1 was present in a TGN38 positive compartment at 2 hours and increased at 3 hours (Figure 9B). When synaptotagmin1 and TGN38 co-localized then NPY-mCherry was often also found on the same location. This shows that some endocytosed synaptotagmin1 might be recycled to LDCVs through the TGN.

Further, we examined whether LDCVs contain a mixture of freshly endocytosed (E) synaptotagmin, and non-cycling (NC) synaptotagmin1 comprising de novo generated synaptotagmin1 and or synaptotagmin1 located on LDCVs that were not exo- endocytosed during the experiment. This required labeling synaptotagmin1 as it was endocytosed from living cells, and again when the cells were fixed and permeabilized. To discriminate between the two reactions, we marked the anti-synaptotagmin1 antibody that was taken up by the cells through endocytosis with Alexa 488 labeled secondary antibody. All the remaining unrecognized epitopes of the primary antibody were then blocked with Fab fragments anti-rabbit IgG (Table 1). The following round of staining with the same primary anti-synaptotagmin1 and secondary antibody Alexa 647 anti-rabbit was performed to mark the non-cycling pool of synaptotagmin1 (for more details see material and methods). Very few vesicles appear white on the overlay images of representative cells indicating that few NPY-mCherry loaded LDCVs contained E- and NC-synaptotagmin1 (Figure 9C). Counting the number of puncta in which NPY-mCherry was co-localized to E-synaptotagmin1 or
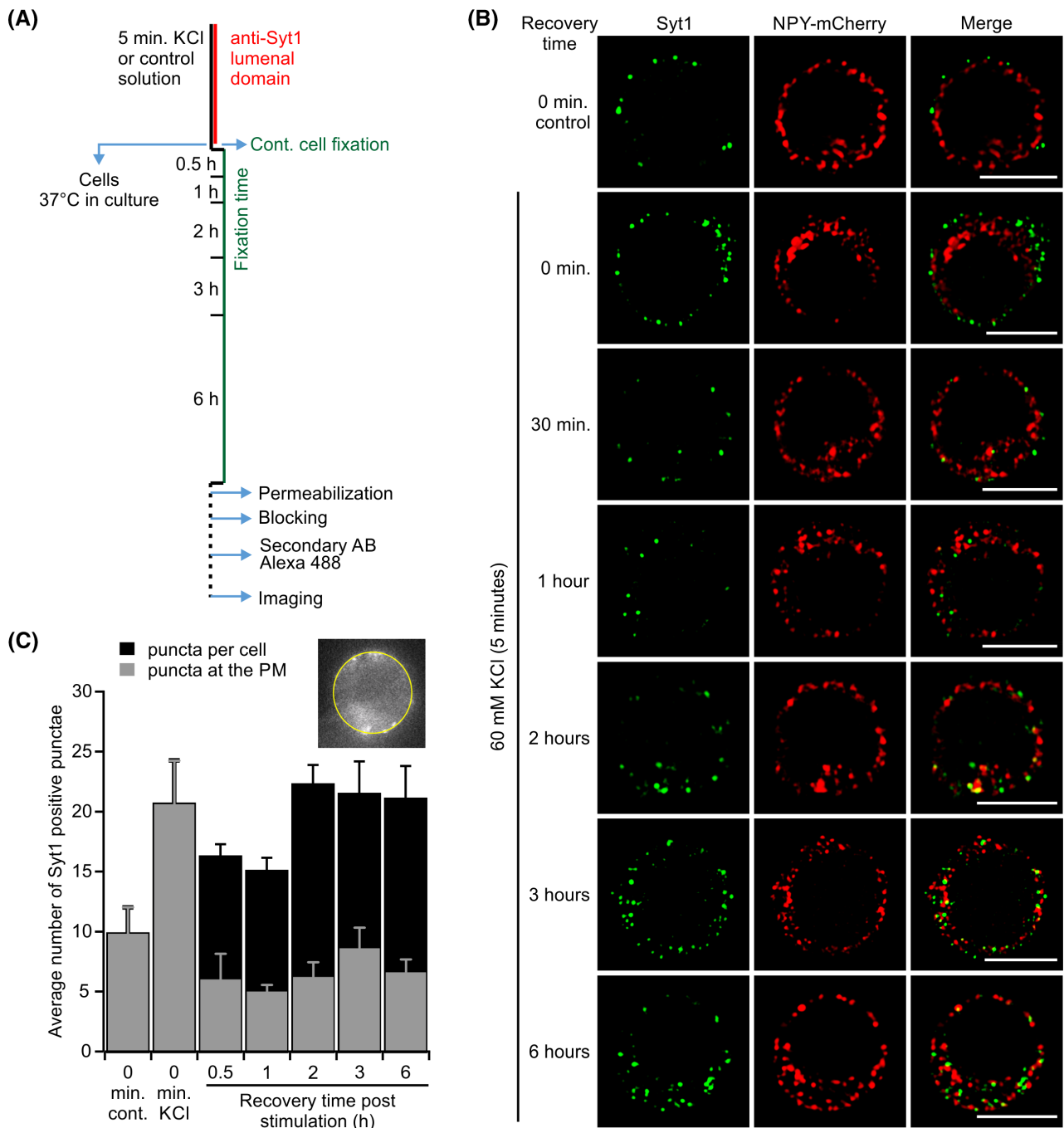
FIGURE 8 Endocytosis of synaptotagmin1. Endocytosis of synaptotagmin1 was examined in NPY-mCherry overexpressing cells. A, Schematic representation of the protocol used to label recycling synaptotagmin1. Cells were incubated at 1:200 in 60 mM KCl/control (normal extracellular) solution for 5 minutes together with anti-synaptotagmin1 lumenal domain antibody. Control cells were fixed after 5 minutes and the remaining cells were allowed to recover at 37°C with 13% CO_2 for various times before fixation. B, Representative single plane SIM images of the endocytosed synaptotagmin1 (green) and NPY-mCherry signal (red). The recovery time after stimulation is indicated on the left. Scale bars: 5 μm. C, Analysis of the number of synaptotagmin1 puncta on either the entire central slice of the cell (black) or at the cell's periphery (PM, gray) at varying recovery time post stimulation. For the latter we counted synaptotagmin1 positive puncta touching the border of the region of interest, which is shown as yellow circle on the inset, and that delimited the plasma membrane (n = 5 cells for each time point). Note that on the time points 0 min the numbers of puncta at the plasma membrane and in the entire cell slice were the same

NC-synaptotagmin1 showed that at least five times more LDCVs contained only NC-synaptotagmin1 than only E-synaptotagmin1 (Figure 9D). Moreover, half as many LDCVs contained both E- and NC-synaptotagmin1 as compared to LDCVs containing only E-synaptotagmin1 (Figure 9C). Finally, 5.6 ± 0.7 LDCVs (n = 5) contained both E- and NC-synaptotagmin1 but no NPY-mCherry indicating
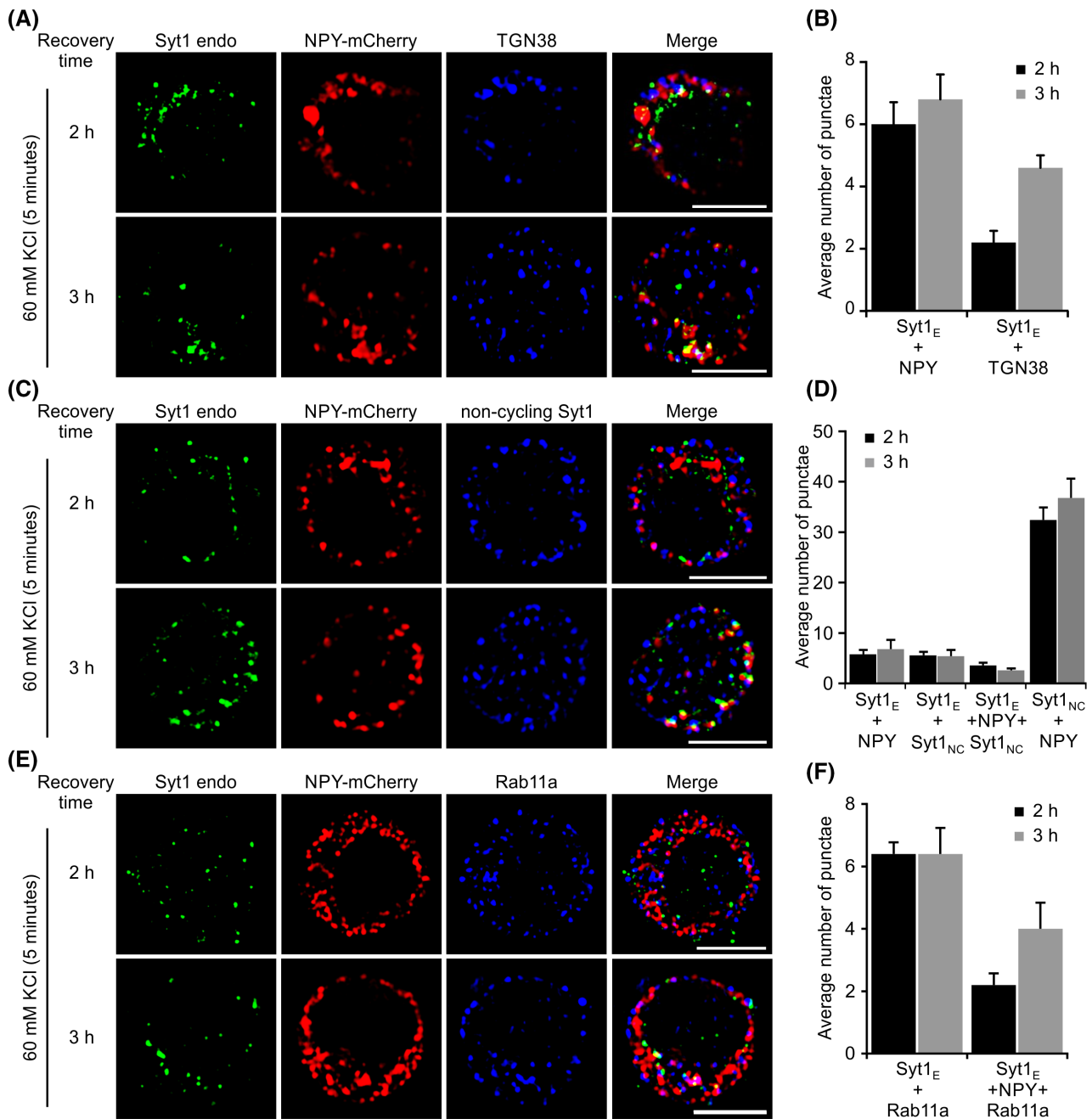
FIGURE 9 Endocytosed synaptotagmin1 is found on LDCVs and can mix with a non-cycling pool of synaptotagmin1. Endocytosis of synaptotagmin1 (Syt1, green) observed in NPY-mCherry (red) overexpressing cells that were stimulated with 60 mM KCl for 5 minutes in presence of 1:200 anti-synaptotagmin1 lumenal domain antibody, co-immunolabeled with anti-TGN38 antibody, A, anti-synaptotagmin1, C, or anti-Rab11A antibody, E. Cells were maintained at rest to recover for 2 and 3 hours after stimulation. Displayed are single plane images acquired by SIM. Scale bars: 5 μm. B, Analysis of the number of endocytosed synaptotagmin1 (Syt_E) vesicles that were also positive for NPY-mCherry alone or with TGN38. D, Analysis of the number of endocytosed synaptotagmin1 (Syt_E) puncta that coincided with vesicles containing only NPY-mCherry, only non-cycling synaptotagmin1 (Syt_{NC}), and vesicles containing both (n = 5 cells for each time point). F, Analysis of the number of endocytosed synaptotagmin1 (Syt_E) that were positive for anti-Rab11 alone or together with NPY-mCherry. For B, D and F, n = 5 cells for each time point

that the fusion of endosomes containing E-synaptotagmin1 with vesicle containing NC-synaptotagmin1 occurs before fusing with LDCV-precursor.

Lastly, we investigated which route endocytosed synaptotagmin1 takes during recycling by examining co-localization with recycling endosome marker Rab11A. The experimental design was the same as the co-localization experiment of endocytosed synaptotagmin1 and TGN38. As can be seen on the images of representative cells after 2 or 3 hours of recovery virtually no co-localization between endocytosed synaptotagmin1 and Rab11A is visible (Figure 9E). Single

TABLE 1 Details of different antibodies used in the study

No.	Antibody	Immunogen	Manufacturer and catalog no.	Working dilution
1	Anti-CgA	Recombinant fragment from the C-terminal (Human)	Abcam (ab15160)	1:1000
2	Anti-LAMP1	NIH/3 T3 mouse embryo fibroblast tissue culture cell membranes	Developmental studies hybridoma bank (1D4B)	1:500
3	Anti-GM130	Rat GM130 aa. 869-982	BD Biosciences (610823)	1:100
4	Anti-TGN38	Recombinant protein corresponding to extracellular domain of TGN38 (Figure 3). Synthetic peptide from the cytoplasmic part of mouse TGN46, conjugated to an immunogenic carrier protein (Figure 7).	AbD Serotec (AHP1597) Abcam (ab76282)	1:100 1:100
5	Anti-syntaxin6	Recombinant rat syntaxin6 fusion protein. Recognized epitope is N-term residues 1–25	Abcam (ab12370) Clone 3D10	1:500
6	Anti-Rab11	Synthetic peptide corresponding to Human Rab11A aa 150 to the C-terminus	Abcam (ab128913)	1:100
7	Anti-synaptobrevin2	Synthetic peptide SATAATVPPA-APAGEG (aa 2-17 in rat synaptobrevin2) coupled to key-hole limpet hemocyanin via an added N-terminal cysteine residue.	Synaptic System (104211)	1:1000
8	Anti-cellubrevin	Recombinant protein of the cytoplasmic part of rat cellubrevin (aa 1-81).	Synaptic System (104103)	1:1000
9	Anti-synaptotagmin1 (C)	Recombinant protein matching AA 80 to 421 from rat synaptotagmin1	Synaptic System (105011)	1:400
9	Anti-synaptotagmin1 (L)	Synthetic peptide MVSASRPE (aa 1-8 in mouse synaptotagmin1) coupled to key-hole limpet hemocyanin via an added C-terminal residue.	Synaptic System (105102)	1:2000 and 1:200
10	Alexa 488 phalloidin	High affinity filamentous actin probe conjugated with green fluorescent Alexa fluor 488 dye.	Life technologies, Invitrogen (A-12379)	2.5%
	Secondary antibody		Life technologies, Invitrogen	
11	Alexa 488	goat anti-mouse	A-11001	1:2000
12	Alexa 647	goat anti- mouse	A-21235	1:2000
13	Alexa 488	goat anti-rabbit	A-11008	1:2000
14	Alexa 647	goat anti-rabbit	A-21244	1:2000
15	Fab fragments	Goat anti-mouse (IgG H&L)	Biomol: Rockland, (810-1102)	1:50

plane analysis of acquired cells showed that 6.4 ± 0.9 Rab11A vesicles were positive for endocytosed synaptotagmin1 (Figure 9F; n = 5). This indicated that recycling of synaptotagmin1 is likely independent of Rab11A.

3 | DISCUSSION

We followed LDCV biogenesis using overexpression of NPY tagged to the fluorescent protein mCherry to label newly generated LDCVs in combination with immunofluorescence and SIM. We found that LDCVs originate from an intermediate Golgi compartment that does not contain the classical cis- or trans-Golgi marker GM130 or TGN38 (Figure 10), thereby confirming data obtained in PC12 cells.[2] Our data indicate that this compartment is rather the syntaxin6 positive TGN sub-compartment corroborating previous studies that showed that it is involved in LDCV biogenesis.[2,9] Association of these immature

LDCVs with the exocytotic machinery composed of synaptobrevin2, cellubrevin and synaptotagmin1 occurs at a late stage when LDCVs have already exited the Golgi (Figure 10). Indeed, after 2 hours of transfection, while all the NPY-mCherry is still exclusively localized to the Golgi, virtually no co-localization with any of these membrane proteins could be measured. Co-localization indices increase as vesicles exit the Golgi and 1 hour later ∼30% of NPY-mCherry loaded vesicles are clearly associated with these membrane proteins. This result is in contradiction with findings in PC12 cells[2] but agrees with work performed on mouse chromaffin cells.[8,9] The loading of LDCVs with the exocytotic machinery renders them potentially fusion competent and coincides with their redistribution to the cytoplasm or the plasma membrane. This confirms previous findings showing that in bovine chromaffin cells exocytosis of NPY-mRFP labeled LDCVs can be exocytosed as early as 12 hours post transfection[19] but undermines the hypothesis that 1 day of maturation is necessary for newly generated LDCVs to become fully functional.[8,9]
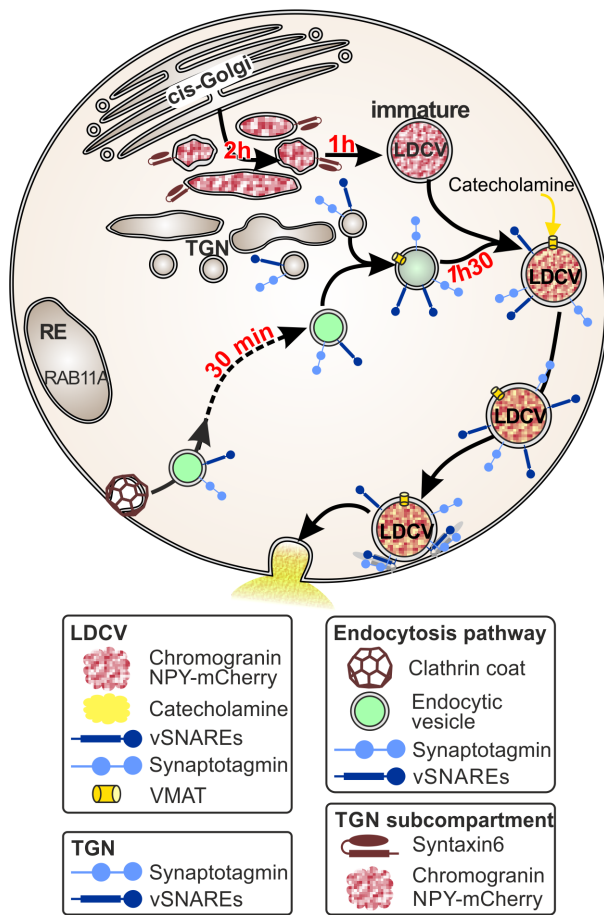
FIGURE 10 Model of LDCV biogenesis in mouse chromaffin cells. NPY is processed within 3 hours of synthesis to fully functional LDCV. The maturation pathway involves a syntaxin6 positive sub-compartment of the TGN. LDCV membrane proteins are added to LDCVs at a late stage after NPY has already been packed in immature vesicles. The exocytosis machinery (vSNARES and synaptotagmin1) is presumably taken up by clathrin-mediated endocytosis and then recycled within 2 hours to LDCVs. These freshly endocytosed membrane proteins can mix with proteins from a non-cycling pool

In addition, we showed by following with the recycling of synaptotagmin1 that proteins of the exocytotic machinery can originate from de novo synthesis or from recycling after a round of exo- and endocytosis. Whether de novo synthesized or recycled proteins are preferentially sorted to new LDCVs is still unknown and cannot be addressed with our experimental design. In our experimental approach we label with recycling anti-synaptotagmin1 antibody only the synaptotagmin that was exocytosed during the time of the stimuli. However, a large portion of the cell's LDCVs are not being released and they will all be labeled only with non-cycling anti-synaptotagmin1 matching the fact that about 80% of all NPY-mCherry positive vesicle were labeled only with non-cycling anti-synaptotagmin1. They are then undiscernible from vesicles made after the start of the experiment containing de-novo synthetized synaptotagmin1. Nevertheless, we found that a number of LDCVs containing NPY-mCherry were only positive for endocytosed synaptotagmin1. Thus, fusion of

endosome containing synaptotagmin1 with precursor vesicles containing de novo synthesized synaptotagmin1 is not a required step to generate mature LDCVs. Finally, endocytosed synaptotagmin1 required about 2 hours to be recycled to NPY-mCherry marked LDCVs. Previous work found that Glycoprotein III/clusterin, a LDCV membrane protein, is recycled to vesicles with electron dense content within 45 minutes but needed another 6 hours to move to classical LDCVs in bovine chromaffin cells.[4] Hence, recycling of LDCV membrane is faster in mouse chromaffin cells than in bovine chromaffin cells. Our data also implies that recycled synaptotagmin1 needs at least 2 hours to be exocytosed again and agrees well with the fact that vesicles loaded with recycling synaptotagmin1 could not be released within 1 hour of endocytosis.[9] However, the minimum delay between endocytosis of synaptotagmin1 and a new round of exocytosis still needs to be determined. The recycling pathway encompasses a variety of specialized membrane compartments.[20,21] We showed that synaptotagmin1 recycling is probably independent of Rab11A positive recycling endosome. It will be of interest to determine through which endosomal pathway endocytosed synaptotagmin and vSNAREs are traveling and whether they use the same route.

The question now is where the association between NPY-mCherry loaded vesicles and membrane-bound exocytotic proteins takes place. Vesicles loaded with only NPY-mCherry could be observed in a triple staining with NPY-mCherry, anti-synaptobrevin2 and anti-cellubrevin 24 hours after transfection. Therefore, it is very likely that the vSNAREs as well as synaptotagmin1 are inserted in the membranes of LDCVs via fusion of two precursor vesicles, one directly coming from the Golgi containing the peptides (NPY, chromogranin etc.) and another one containing the vesicular proteins originating from recycling or from de novo synthesis (Figure 10). This aspect of mouse chromaffin cell LDCV biogenesis is very similar to LDCV biogenesis in PC12 cells, in which fusion of precursor vesicles during LDCV maturation has been described albeit at a much slower time scale.[22] Interestingly, this fusion required syntaxin6 and synaptotagmin IV[23] agreeing with our finding, which suggested that LDCVs bud from a syntaxin6 positive TGN sub-compartment.[9,24] In *Caenorhabditis elegans* sensory neurons the syntaxin6 positive compartment has proven to constitute a quality control step for the biogenesis of LDCVs after exiting the TGN.[25] The pathway described here cannot be generalized to all LDCVs membrane proteins. For example, in AtT-20 corticotrope tumor cells integral LDCVs membrane proteins such as the carboxypeptidase D or the peptidylglycine α-amidating monooxygenase are processed together with the LDCV content (pro-opiomelanocortin/ACTh) throughout the entire cis- and trans-Golgi network to finally bud as immature granule.[26,27] Only afterwards some components like the carboxypeptidase D are removed from the immature granule to join a constitutive secretion pathway. Shedding of LDCV membrane proteins have also been described in PC12[23] but they do not appear to enter a constitutive secretion pathway.

Vesicles freshly packed with NPY-mCherry remained near the Golgi for about 1 hour (Figure 10) very similarly to what has been shown in PC12 cells.[3] These immature LDCVs move toward the

plasma membrane but, contrary to findings in PC12 cells, they do not appear to be retained at the plasma membrane[3] (Figure 10). The number of LDCVs in close apposition to the plasma membrane remained stable over time while the number of LDCVs located in the inner ring of the cortical actin network increased to reach a plateau within the first 6 hours after transfection. This confirms previous finding in bovine chromaffin cells showing that in resting cells LDCVs are not primarily retained at the plasma membrane by tethering or docking mechanisms but rather because they become trapped in the F-actin meshwork that covers the plasma membrane ([28-30] and for detailed review see[31]). Finally, the number of LDCVs in the cytoplasm away from the plasma membrane increased steadily over time. This finding contradicts a model of age-dependent distribution of vesicles in bovine chromaffin cells, which suggested that the youngest LDCVs are found in close proximity to the plasma membrane whereas older LDCVs are located toward the cell interior.[32] However, this model was mainly based on a study in which the age of secreted LDCVs was investigated using dsRed-E5, which changes its emission from green to red over 16 hours.[33] Thus, the time scale in which this age-dependent redistribution and secretion of LDCVs was studied is very different to our current work, and might explain the discrepancy.

4 | CONCLUSION

Our investigation of large dense core vesicle biogenesis in chromaffin cells demonstrated that precursor vesicles exit a trans-Golgi sub-compartment, fuse with vesicles containing the exocytosis machinery before moving to the plasma membrane. Furthermore, we showed that recycling of synaptotagmin1 is independent of Rab11A positive recycling endosome and takes about 2 hours to be fulfilled. With this work we show that LDCV biogenesis of mouse chromaffin cells and PC12, which are derived from pheochromocytoma of the rat adrenal medulla and often serve as model for neuroendocrine cell, display many similarities. However, we also uncovered important differences which highlight's the caution one should use comparing both type of cells. We have integrated our data in a timed model of LDCV biogenesis (Figure 10) providing an important framework for future work on exocytosis in mouse chromaffin cells.

5 | MATERIALS AND METHODS

5.1 | Chromaffin cell preparation and electroporation

All experiments were performed on mouse adrenal medullary chromaffin cells in primary culture. The cells were prepared from postnatal day 3 black 6 (C57Bl/6N) mice pups of either sex. Cell culture was based on the method described in Reference[34]. In short, pups were decapitated and adrenal glands were rapidly removed, placed in Locke's solution and cleaned from blood, connective tissue and fat.

Then the glands were incubated for 20 minutes in DMEM containing 20 U/mL papain (Worthington, Lakewood, New Jersey). After removal of the papain solution, the glands were washed in an inactivating solution (DMEM plus 10% BSA) for 4 minutes followed by mechanical trituration to become a cell suspension. The cells were then electroporated with the Neon Transfection System (Life technologies, Invitrogen, Darmstadt, Germany)[12,35] using the following procedure. They were centrifuged twice at 4000 rpm for 5 minutes. At first the cells were suspended in 500 μL Dulbecco's phosphate-buffered saline and then they were suspended in 20 μL of the proprietary R-buffer provided in the electroporation kit. Then, 4 μg of endofree plasmid construct pMAX-NPY-mCherry was added and well mixed with the cells. For each 10 μL electroporation, cells were subjected to 1 pulse of 1400 V with 30 ms pulse width. Cells were then added to DMEM supplemented with 1% ITS-X (Thermofisher/Gibco) and 0.4% of penicillin/streptomycin (10 000 U/mL, Fischer Scientific) and were plated on collagen (Rat tail collagen, BD Biosciences, Heidelberg, Germany) coated coverslips and allowed to settle for 30 minutes. After 30 minutes, 3 mL of DMEM was added to each well. Cells were maintained in culture at 37°C with 13% CO2 for various time post transfection. DMEM and Dulbecco's phosphate-buffered saline were from Life technologies, Invitrogen, Darmstadt, Germany. All experiments were performed in compliance with the guidelines for the welfare of experimental animals issued by the Federal Government of Germany and the State of Saarland.

pMAX NPY-mCherry plasmid[12] includes the NPY-mCherry construct #67156 from Addgene subcloned in a pMAX vector (Lonza GmbH) with improved multiple cloning site using NheI and EcoRV as restriction sites. The final plasmid size was 3895 bp with NPY-mCherry. The construct was verified by DNA sequencing.

5.2 | Immunocytochemistry

Cells were washed twice in PBS and fixed in 4% paraformaldehyde (Merck, KGaA, Darmstadt, Germany) for 20 minutes at room temperature, followed by 10 minutes 50 mM Glycine quenching step. Then they were permeabilized with 0.1% Triton-X-100/2.5% NGS (normal goat serum, Life technologies, Invitrogen, Darmstadt, Germany)/PBS (made in-house), and blocked with 2.5% NGS/PBS. After blocking, the cells were incubated with primary antibody diluted with blocking solution for 1 hour and with secondary antibody for 45 minutes. Coverslips were mounted on microscope slides with 20 μL of mounting medium. For the biogenesis experiment, chromaffin cells were fixed at different time points starting from 2 hours post transfection up to 24 hours. Then, 2.5% phalloidin-Alexa488 (Invitrogen, Darmstadt, Germany) was applied to the cells with the secondary antibody to label the actin beneath the plasma membrane. Detailed description of the antibodies origin and usage conditions are given in Table 1. Glycine and Triton-X-100 were from Roth, Karlsruhe, Germany.

Immunolabeling with two antibodies raised against same species was done by using Fab fragments against the same species. In brief,

first antibody labeling was done as mentioned above. Then after PBS washing, the cells were blocked again with 2.5% NGS/PBS for 1 hour at room temperature. Then washed three times with PBS and cells were incubated with affinity Fab fragments (1:50 dilution in 2.5% NGS/PBS) for 1 hour at room temperature. Then cells were washed three times with PBS for 10 minutes each, the secondary antibody was applied and the protocol mentioned above was followed.

5.3 | Endocytosis experiment

Chromaffin cells were maintained in culture 24 hours post transfection. Cells were washed once in PBS. Polyclonal anti-synaptotagmin1 lumenal domain antibody was used to study the recycling of synaptotagmin1. Specificity of this antibody was tested by performing immunolabeling in synaptotagmin1 WT and KO cells. Antibody was diluted with a factor of 1:200 in normal extracellular solution (control solution in mM: 152 NaCl, 2.4 KCl, 10 HEPES, 1.2 $MgCl_2$, 2.5 $CaCl_2$, 10 glucose at pH = 7.4.) and 60 mM KCl (depolarizing solution in mM: 94.4 NaCl, 60 KCl, 10 HEPES, 1.2 $MgCl_2$, 2.5 $CaCl_2$, and 10 glucose at pH = 7.4). Cells were incubated in these solutions for 5 minutes at room temperature. Some cells were fixed immediately thereafter. Remaining cells were incubated at 37°C with 13% CO2 and were fixed 30 minutes, 1, 2, 3 and 6 hours after stimulation. Immunolabeling protocol was as described before. NaCl, $MgCl_2$, $CaCl_2$, Glucose and KCl were from Merck, Darmstadt, Germany.

In co-staining experiments, first the endocytosis experiment was carried out followed by permeabilization, blocking, second primary antibody application, and then secondary antibody for both markers was applied. In co-staining experiments involving antibodies raised in the same species, first the protocol for single antibody labeling was used followed by the application of Fab fragments and then the second antibody was applied and the above-mentioned immunolabeling protocol was followed.

5.4 | Structured illumination microscopy

The acquisition of all images was performed using high-resolution structured illumination microscopy (SIM; Elyra PS.1 Zeiss, Göttingen, Germany[36]) equipped with ×63, 1.4 NA Plan-apochromatic objective. Excitation wavelengths used were 488, 561 and 635 nm and optimal grating was selected automatically by the acquisition software. SIM illumination mode was set to five phases × five rotations to obtain maximal resolution. Gaussian fit of SIM Images of 40 nm crimson red beads gave a half width at half maximum of 76 ± 12 nm in X, Y and 246 ± 53 nm in Z (Figure S1A). Z-stacks of entire cells were obtained with 200 nm interval between slices. Acquisition and SIM processing was done with ZEN 2010 software (Zeiss, Göttingen, Germany). Comparing SIM and STED images of the same cell shows that SIM resolution in XYZ was good enough to be able to identify individual LDCVs (Figure S1B,C).

5.5 | Distance analysis, co-localization analysis and statistics

Analysis of the distance between center of vesicle to the boundary of the Golgi and plasma membrane was done by using in-house written software. With the help of the software the boundaries of plasma membrane and Golgi were marked sequentially and then each vesicle was marked manually. Next the software measured the shortest possible distance between the vesicle center and Golgi/plasma membrane (for more details see reference[12]). The values were then imported to IgorPro software to make the histograms. Pearson's and Manders co-localization analysis was done by using the JACoP plugin[37] in ImageJ 1.47f (http://imagej.nih.gov/ij/) on one single plane per cell. Analysis at the Golgi was done by first marking the area around the Golgi manually, cropping to the selected area and then analyzing the co-localization. Statistical analysis was done with Student's t test because data passed normality test using Sigma Plot (Systat Software Inc., San Jose, California).

CONFLICT OF INTEREST
The authors declare no competing financial interests.

PEER REVIEW
The peer review history for this article is available at https://publons.com/publon/10.1111/tra.12783.

ORCID
Ute Becherer https://orcid.org/0000-0001-6005-7517

REFERENCES

1. Crivellato E, Nico B, Ribatti D. The chromaffin vesicle: advances in understanding the composition of a versatile, multifunctional secretory organelle. *Anat Rec (Hoboken)*. 2008;291(12):1587-1602. https://doi.org/10.1002/ar.20763.
2. Park JJ, Gondre-Lewis MC, Eiden LE, Loh YP. A distinct trans-Golgi network subcompartment for sorting of synaptic and granule proteins in neurons and neuroendocrine cells. *J Cell Sci*. 2011;124(Pt 5):735-744. https://doi.org/10.1242/jcs.076372.
3. Rudolf R, Salm T, Rustom A, Gerdes HH. Dynamics of immature secretory granules: role of cytoskeletal elements during transport, cortical restriction, and F-Actin-dependent tethering. *Mol Biol Cell*. 2001;12(5):1353-1365.
4. Patzak A, Winkler H. Exocytotic exposure and recycling of membrane antigens of chromaffin granules: ultrastructural evaluation after immunolabeling. *J Cell Biol*. 1986;102(2):510-515.
5. Tooze SA, Huttner WB. Cell-free protein sorting to the regulated and constitutive secretory pathways. *Cell*. 1990;60(5):837-847.
6. Elias S, Delestre C, Courel M, Anouar Y, Montero-Hadjadje M. Chromogranin A as a crucial factor in the sorting of peptide hormones to secretory granules. *Cell Mol Neurobiol*. 2010;30(8):1189-1195. https://doi.org/10.1007/s10571-010-9595-8.

7. Estevez-Herrera J, Pardo MR, Dominguez N, Pereda D, Machado JD, Borges R. The role of chromogranins in the secretory pathway. *Biomol Concepts*. 2013;4(6):605-609. https://doi.org/10.1515/bmc-2013-0020.

8. Pinheiro PS, Jansen AM, de Wit H, et al. The BAR domain protein PICK1 controls vesicle number and size in adrenal chromaffin cells. *J Neurosci*. 2014;34(32):10688-10700. https://doi.org/10.1523/JNEUROSCI.5132-13.2014.

9. Walter AM, Kurps J, de Wit H, et al. The SNARE protein vti1a functions in dense-core vesicle biogenesis. *EMBO J*. 2014;33(15):1681-1697. https://doi.org/10.15252/embj.201387549.

10. Bost A, Pasche M, Schirra C, Becherer U. Super-resolution microscopy in studying neuroendocrine cell function. *Front Neurosci*. 2013; 7:222. https://doi.org/10.3389/fnins.2013.00222.

11. Schermelleh L, Carlton PM, Haase S, et al. Subdiffraction multicolor imaging of the nuclear periphery with 3D structured illumination microscopy. *Science (New York, NY)*. 2008;320(5881):1332-1336. https://doi.org/10.1126/science.1156947.

12. Hugo S, Dembla E, Halimani M, Matti U, Rettig J, Becherer U. Deciphering dead-end docking of large dense core vesicles in bovine chromaffin cells. *J Neurosci*. 2013;33(43):17123-17137. https://doi.org/10.1523/JNEUROSCI.1589-13.2013.

13. Pasche M, Matti U, Hof D, Rettig J, Becherer U. Docking of LDCVs is modulated by lower intracellular [Ca^{2+}] than priming. *PLoS One*. 2012; 7(5):e36416.

14. Merzlyak EM, Goedhart J, Shcherbo D, et al. Bright monomeric red fluorescent protein with an extended fluorescence lifetime. *Nat Methods*. 2007;4(7):555-557. https://doi.org/10.1038/nmeth1062.

15. Shaner NC, Campbell RE, Steinbach PA, Giepmans BN, Palmer AE, Tsien RY. Improved monomeric red, orange and yellow fluorescent proteins derived from Discosoma sp. red fluorescent protein. *Nat Biotechnol*. 2004;22(12):1567-1572.

16. Greaves J, Carmichael JA, Chamberlain LH. The palmitoyl transferase DHHC2 targets a dynamic membrane cycling pathway: regulation by a C-terminal domain. *Mol Biol Cell*. 2011;22(11):1887-1895. https://doi.org/10.1091/mbc.E10-11-0924.

17. Stephens DJ, Banting G. Direct interaction of the trans-Golgi network membrane protein, TGN38, with the F-Actin binding protein, neurabin. *J Biol Chem*. 1999;274(42):30080-30086.

18. Borisovska M, Schwarz YN, Dhara M, et al. Membrane-proximal tryptophans of synaptobrevin II stabilize priming of secretory vesicles. *J Neurosci*. 2012;32(45):15983-15997. https://doi.org/10.1523/JNEUROSCI.6282-11.2012.

19. Nofal S, Becherer U, Hof D, Matti U, Rettig J. Primed vesicles can be distinguished from docked vesicles by analyzing their mobility. *J Neurosci*. 2007;27(6):1386-1395.

20. Le Roy C, Wrana JL. Clathrin- and non-clathrin-mediated endocytic regulation of cell signalling. *Nat Rev Mol Cell Biol*. 2005;6(2):112-126. https://doi.org/10.1038/nrm1571.

21. Scott CC, Vacca F, Gruenberg J. Endosome maturation, transport and functions. *Semin Cell Dev Biol*. 2014;31:2-10. https://doi.org/10.1016/j.semcdb.2014.03.034.

22. Tooze SA, Flatmark T, Tooze J, Huttner WB. Characterization of the immature secretory granule, an intermediate in granule biogenesis. *J Cell Biol*. 1991;115(6):1491-1503.

23. Ahras M, Otto GP, Tooze SA. Synaptotagmin IV is necessary for the maturation of secretory granules in PC12 cells. *J Cell Biol*. 2006;173 (2):241-251. https://doi.org/10.1083/jcb.200506163.

24. Wendler F, Page L, Urbe S, Tooze SA. Homotypic fusion of immature secretory granules during maturation requires syntaxin 6. *Mol Biol Cell*. 2001;12(6):1699-1709.

25. Laurent P, Ch'ng Q, Jospin M, Chen CC, Lorenzo R, de Bono M. Genetic dissection of neuropeptide cell biology at high and low activity in a defined sensory neuron. *Proc Natl Acad Sci U S A*. 2018;115 (29):E6890-E6899. https://doi.org/10.1073/pnas.1714610115.

26. Kalinina E, Varlamov O, Fricker LD. Analysis of the carboxypeptidase D cytoplasmic domain: implications in intracellular trafficking. *J Cell Biochem*. 2002;85(1):101-111. https://doi.org/10.1002/jcb.10112.

27. Bonnemaison M, Back N, Lin YM, Bonifacino JS, Mains R, Eipper B. AP-1A controls secretory granule biogenesis and trafficking of membrane secretory granule proteins. *Traffic (Copenhagen, Denmark)*. 2014;15(10):1099-1121. https://doi.org/10.1111/tra.12194.

28. Neco P, Giner D, Frances MD, Viniegra S, Gutierrez LM. Differential participation of Actin-and tubulin-based vesicle transport systems during secretion in bovine chromaffin cells. *Eur J Neurosci*. 2003;18 (4):733-742. https://doi.org/10.1046/j.1460-9568.2003.02801.x.

29. Papadopulos A, Gomez GA, Martin S, et al. Activity-driven relaxation of the cortical actomyosin II network synchronizes Munc18-1-dependent neurosecretory vesicle docking. *Nat Commun*. 2015;6(1):6297. http://dx.doi.org/10.1038/ncomms7297.

30. Vitale ML, Seward EP, Trifaro JM. Chromaffin cell cortical Actin network dynamics control the size of the release-ready vesicle Pool and the initial rate of exocytosis. *Neuron*. 1995;14(2):353-363. https://doi.org/10.1016/0896-6273(95)90291-0.

31. Li P, Bademosi AT, Luo JC, Meunier FA. Actin remodeling in regulated exocytosis: toward a Mesoscopic view. *Trends Cell Biol*. 2018;28(9): 685-697. https://doi.org/10.1016/j.tcb.2018.04.004.

32. Solimena M, Gerdes HH. Secretory granules: and the last shall be first. *Trends Cell Biol*. 2003;13(8):399-402.

33. Duncan RR, Greaves J, Wiegand UK, et al. Functional and spatial segregation of secretory vesicle pools according to vesicle age. *Nature*. 2003;422(6928):176-180.

34. Liu Y, Schirra C, Edelmann L, et al. Two distinct secretory vesicle-priming steps in adrenal chromaffin cells. *J Cell Biol*. 2010;190(6): 1067-1077. https://doi.org/10.1083/jcb.201001164.

35. Hoerauf WW, Cazares VA, Subramani A, Stuenkel EL. Efficient transfection of dissociated mouse chromaffin cells using small-volume electroporation. *Cytotechnology*. 2015;67(3):573-583. https://doi.org/10.1007/s10616-014-9699-y.

36. Gustafsson MG, Shao L, Carlton PM, et al. Three-dimensional resolution doubling in wide-field fluorescence microscopy by structured illumination. *Biophys J*. 2008;94(12):4957-4970.

37. Bolte S, Cordelières FP. A guided tour into subcellular colocalization analysis in light microscopy. *J Microsc*. 2006;224(Pt 3):213-232. https://doi.org/10.1111/j.1365-2818.2006.01706.x.

SUPPORTING INFORMATION

Additional supporting information may be found online in the Supporting Information section at the end of this article.